Biophysical Journal, Volume *112*

Supplemental Information

Design Rules for Membrane-Embedded Voltage-Sensing Nanoparticles

Kyoungwon Park and Shimon Weiss

Supporting information

Performance Predictions and Design Rules for Membrane-Embedded Semiconducting Voltage-Sensing Nanoparticles

Kyoungwon Park[1] and Shimon Weiss[1,2,3,*]

[1]Dept. of Chemistry & Biochemistry, [2]Dept. of Physiology, [3]California NanoSystems Institute, University of California Los Angeles, Los Angeles CA 90095

SI-1. Parameters used in the calculations

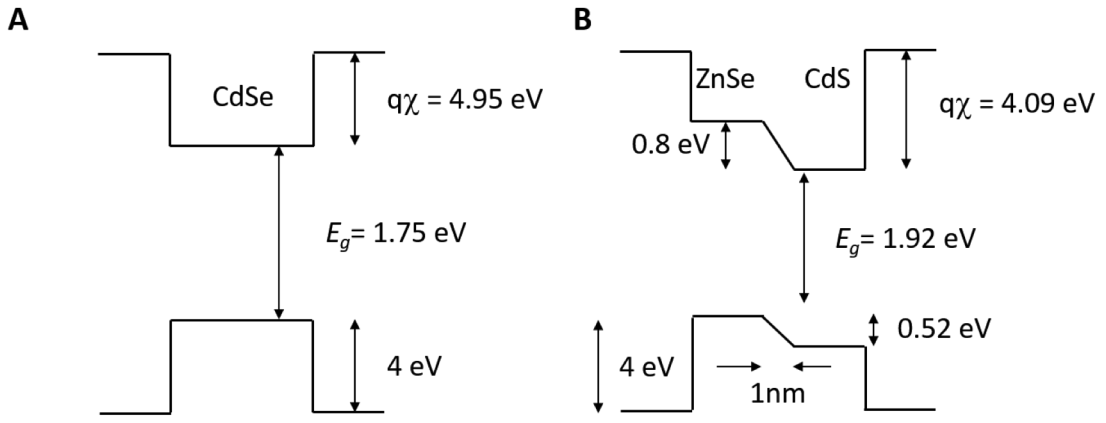

Figure S1. Bandgaps and band offsets parameters for: (A) type-I CdSe NR (B) type-II ZnSe-CdS heterostructure NR (parameters taken from ref. (1)).

	CdSe	ZnSe-CdS
m_e*	0.13(2)	0.21(2)
m_h*	0.45(2)	0.7(2)
ε_r	9.5(2)	8.9(2)
K	20(3)	23(3)

Table S1: Parameters used in the calculations

m_e*, and m_h* are the electron and hole effective masses. ε_r is the dielectric constant. K is the Kane matrix element. Averaged parameters between ZnSe and CdS were calculated and used for the type-II ZnSe-CdS NRs. The energy required to ionize a hole in the valence band of a CdSe NR (in an Auger process) is lowered compared to bulk CdSe due to surface ligands. It is estimated here to be ~1eV (this energy is sensitively dependent on the surface ligand, ranging from 0.1eV for CdSe-3-Mercaptopropionic acid(4) to 2.45eV for CdSE-pyridine(5)). Parameters are taken from refs. 2 and 3.

SI-2. Calculation of the Auger recombination rate

The Fermi-Golden rule was used to calculate the Auger recombination rate according to: $k_A = \frac{1}{\tau_A} = \frac{2\pi}{\hbar}\left|M_{if}\right|^2 \rho(E_f)$, where M_{if} is the Coulomb interaction matrix element. ϱ(E_f) is the density of states at the final state (E_f). We calculated the rate for an Auger electron-hole-hole (ehh) process only. The initial wavefunction is the two-hole wavefunction, written as:

$$\Psi_i(x_1,x_2) = \frac{1}{\sqrt{2}}\psi_h^0(x_1)\psi_h^0(x_2)[\lambda(1)\beta(2) - \lambda(2)\beta(1)]$$

where ψ_h^0 is the hole's ground state. λ and β are the spinors of this state. In the final state, one hole is excited in the valance band continuum and therefore takes the form of a plane wave: $\phi_f(x) = \frac{1}{\sqrt{L}}\exp(ik_f x)$, where L is a normalization factor. The other hole ends up in the conduction band, and therefore can be written as the complex conjugate of the electron's ground state ψ_e^{0*}. The final wavefunction can therefore be written as:

$$\Psi_f(x_1,x_2) = \frac{1}{2}[\psi_e^0(x_1)^*\phi_f(x_2) + \psi_e^0(x_2)^*\phi_f(x_1)][\lambda(1)\beta(2) - \lambda(2)\beta(1)].$$

Having the initial and final states, we can calculate the matrix element.

$$\begin{aligned} M_{if} &= \left\langle \Psi_i \left| V(x_1 - x_2) \right| \Psi_f \right\rangle \\ &= \sqrt{2}\int dx_1 dx_2 \psi_h^0(x_1)^* \psi_h^0(x_2)^* V(x_1 - x_2)\psi_e^0(x_1)^* \phi_f^0(x_2)^* \end{aligned}$$

This integral is calculated according to the procedure described in ref. (6).

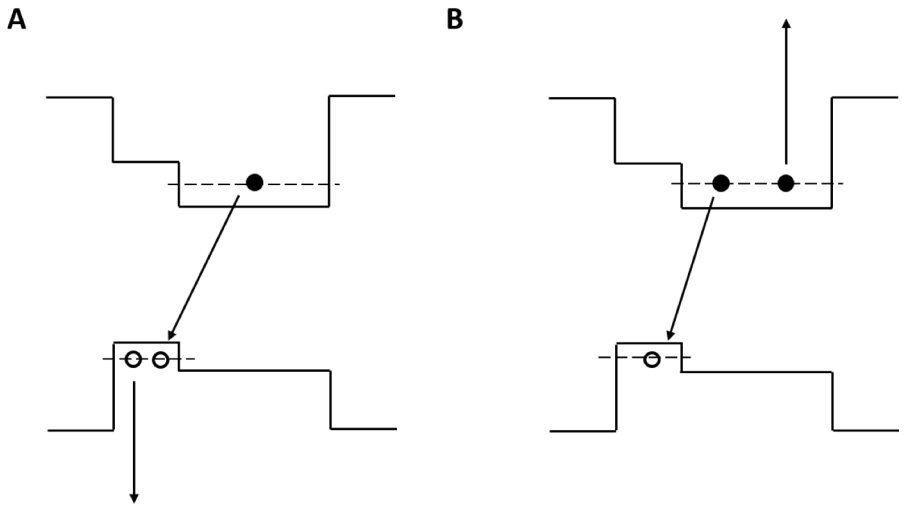

Figure S2. Energy band diagram describing Auger recombination processes: (A) e-h-h scattering (B) e-e-h scattering.

SI-3. Length-dependent Auger rate

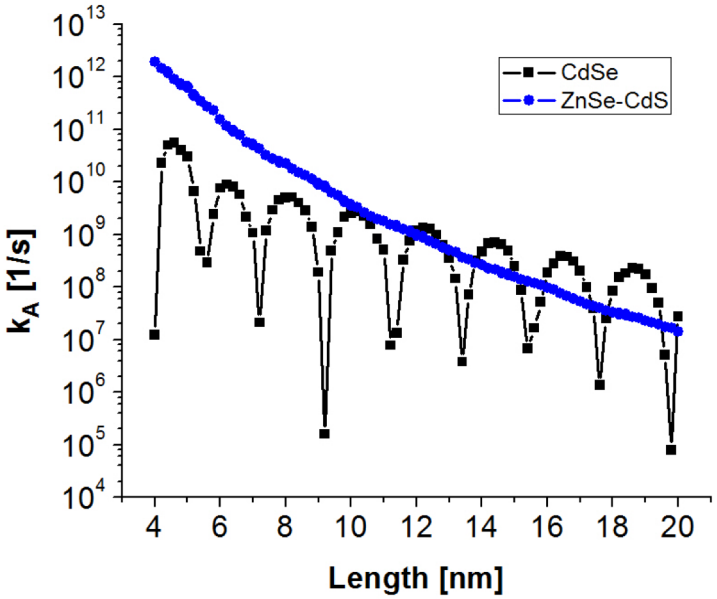

Figure S3. Calculations of the Auger recombination rate as function of the NRs's length for type-I CdSe NRs (black squares) and type-II ZnSe-CdS heterostructure NRs (blue circles).

SI-4. Electric potential profile for different NRs' membrane insertion geometries

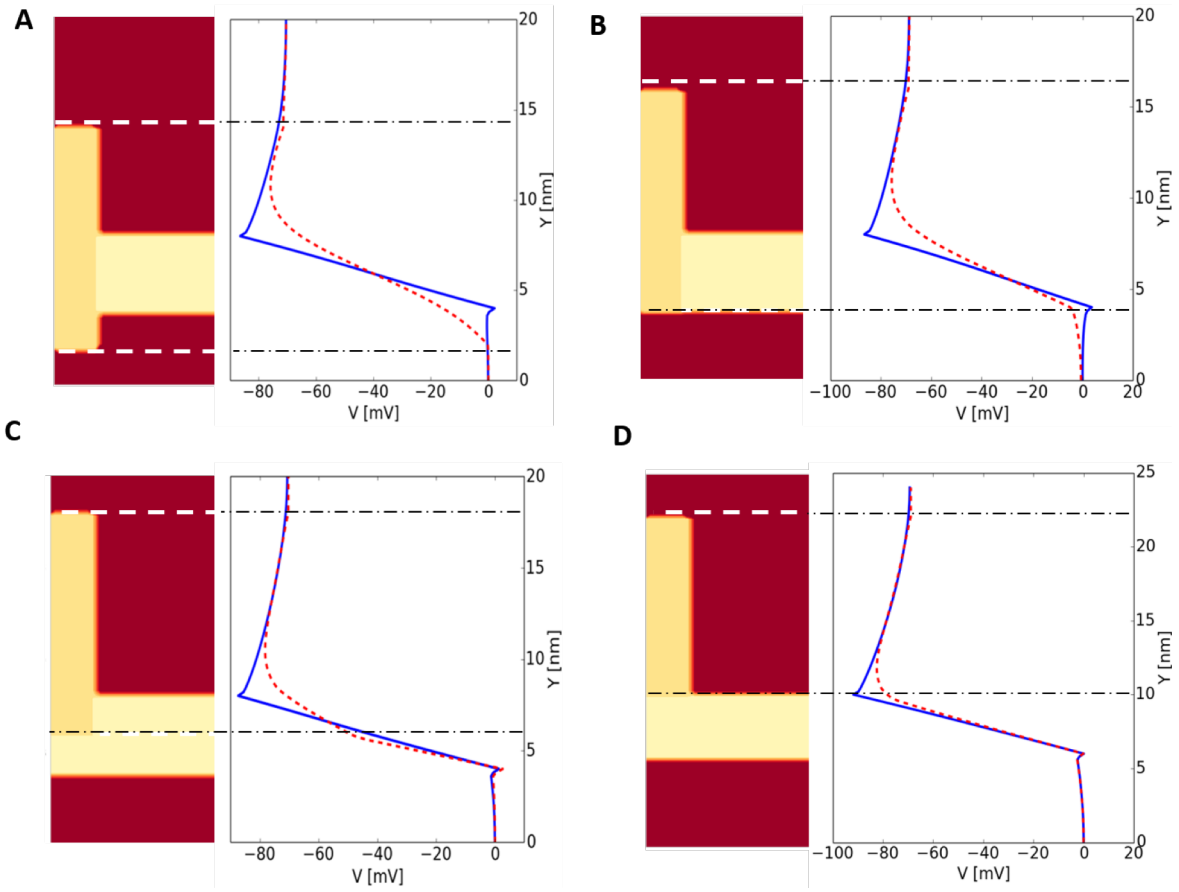

Figure S4. Potential profiles for non-ideally / asymmetrically inserted nanorods.

SI-5. Validating of the linear E-field approximation

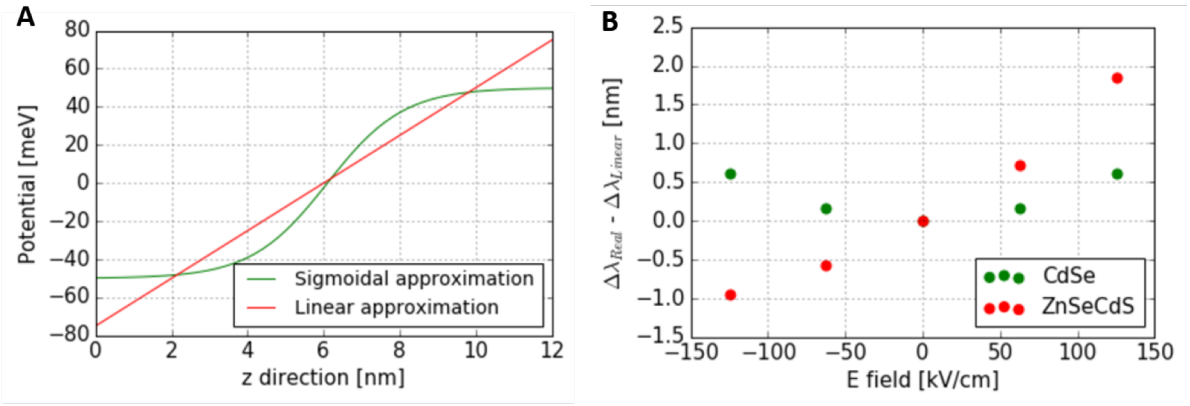

Figure S5. (A) Potential profile along the cylinder axis of a 8nm length's nanorod. Linear approximation (red) and sigmoidal approximation (green). (B) The difference in the Stark shift ($\Delta\lambda$) between the sigmoidal potential calculation ($\Delta\lambda_{Sig}$) and the linear potential calculation ($\Delta\lambda_{Linear}$) for 8 nm long CdSe nanorods (blue dots) and for 8 nm long ZnSe-CdS nanorods (red dots).

In this study, a constant electric field approximation (i.e. the potential is linearly varied) is used to calculate the voltage sensitivity. To incorporate the real potential distribution (Fig. 1C), we need to solve the coupled Schrödinger and Poisson equations with the geometries and dimensions specified in Fig. 1B. However, this requires a ×4 finer mesh, increasing the computation cost by at least a factor of x 16. For this reason, we approximated the external applied electric field to be linear. A more realistic approximation assumes a sigmoidal curve for the potential profile (green curve in Fig. S5):

$$V(z) = \frac{V}{(1+e^{-z})}$$

The differences between the calculated Stark shifts for the sigmoidal and the linear approximations ($\Delta\lambda_{Sig} - \Delta\lambda_{Linear}$) as function of the internal field are plotted in Fig. S5-B. The differences

increases as function of the absolute value of the field for CdSe NRs, and as function of the field for ZnSe-CdS NRs. A 8nm long ZnSe-CdS's $\Delta\lambda_{Linear}$ is 13.7nm at 125 kV/cm, while $\Delta\lambda_{Sigl}$ is 15.5nm for the same voltage (similar to $\Delta\lambda_{Linear}$ at 140 kV/cm). The linear model underestimates the QCSE shift by ~ 10~15%.

SI-6. Dual band intensity ratio for different spectral peak positions (representing heterogeneity)

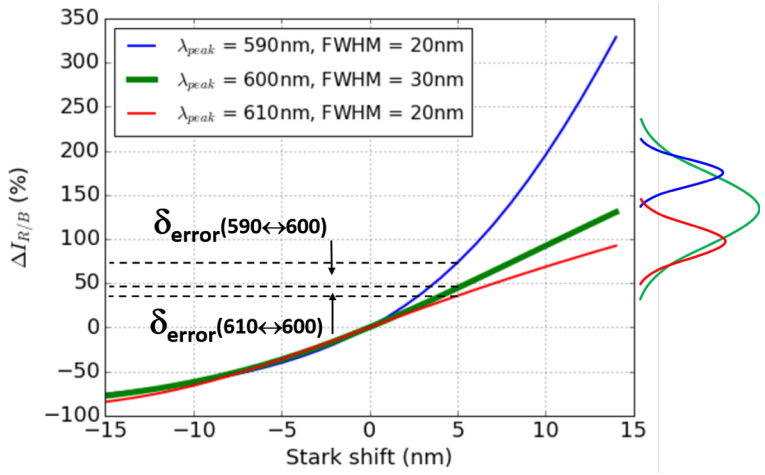

Figure S6. Changes in intensity ratios ($\Delta I_{R/B}$) vs. Stark shifts ($\Delta\lambda$) for ensemble linewidth (λ_{peak} = 600n, FWHM = 30nm, green), single particle linewidth having a smaller core size (λ_{peak} = 590n, FWHM = 20nm, blue), and single particle linewidth having larger core size (λ_{peak} = 610n, FWHM = 20nm, red).

NRs' heterogeneity influences the sensitivity of the dual-view ratiometric intensity measurement. As we defined in eq. (6), the intensity ratio is defined as:

$$I_{R/B}(\Delta\lambda) = \frac{I_R(\Delta\lambda)}{I_B(\Delta\lambda)} = \frac{\int_{600\,\mathrm{nm}}^{\infty} L(\lambda,\Delta\lambda)\,d\lambda}{\int_{-\infty}^{600\,\mathrm{nm}} L(\lambda,\Delta\lambda)\,d\lambda}.$$

We performed this calculation for ensemble linewidth (green) and two single particles' linewidth (blue: smaller core size, red: larger core size) representing inhomogeneous broadening (Fig. S6).

The error in $\Delta I_{R/B}$ is calculated according to: $\delta_{error} = \frac{\Delta I_{R/B}(\Delta\lambda)\big|_{\text{single}} - \Delta I_{R/B}(\Delta\lambda)\big|_{ensemble}}{\Delta I_{R/B}(\Delta\lambda)\big|_{ensemble}}(\%)$.

The measured $\Delta I_{R/B}$ for a Stark blue shift (negative values in the figure), by different size NRs, is hardly impacted by heterogeneity. Reporting a Stark red shift (positive values in the figure), in contrast, is highly disrupted by heterogeneity. For example, a +5nm Stark red shift will be reported by a smaller seed NR having a spectral peak of 590 nm (as compared to a nominal, 600 nm ensemble spectra) with an error of +28%. The same +5nm Stark red shift will be reported by a larger seed NR having a spectral peak of 610 nm (as compared to a nominal, 600 nm ensemble spectra) with an error of -8.7%. This calculation shows that recording with heterogenous particles is possible, but voltage calibration and accuracy of exact voltage determination suffers from heterogeneity. We note that recently, an ensemble FHWM of less than 30 nm has been reported (7) with a single NR's linewidth around ~ 20 nm (8) at room temperature.

Supporting References

1. Dinger, A., S. Petillon, M. Grün, M. Hetterich, and C. Klingshirn. 1999. Conduction band offset of the CdS/ZnSe heterostructure. Semiconductor Science and Technology 14:595.
2. Wang, J., and M. Isshiki. 2007. Wide-Bandgap II–VI Semiconductors: Growth and Properties. In Springer Handbook of Electronic and Photonic Materials. S. Kasap, and P. Capper, editors. Springer US. 325-342.
3. Karazhanov, S. Z., and L. C. Lew Yan Voon. 2005. Ab initio studies of the band parameters of III–V and II–VI zinc-blende semiconductors. Semiconductors 39:161-173.
4. Li, L., G. Tian, Y. Luo, H. Brismar, and Y. Fu. 2013. Blinking, Flickering, and Correlation in Fluorescence of Single Colloidal CdSe Quantum Dots with Different Shells under Different Excitations. The Journal of Physical Chemistry C 117:4844-4851.

5. Kim, B. S., M. A. Islam, L. E. Brus, and I. P. Herman. 2001. Interdot interactions and band gap changes in CdSe nanocrystal arrays at elevated pressure. Journal of Applied Physics 89:8127-8140.
6. Cragg, G. E., and A. L. Efros. 2009. Suppression of Auger Processes in Confined Structures. Nano Letters 10:313-317.
7. Oh, N., S. Nam, Y. Zhai, K. Deshpande, P. Trefonas, and M. Shim. 2014. Double-heterojunction nanorods. Nature Communications 5:3642.
8. Park, K., Z. Deutsch, J. J. Li, D. Oron, and S. Weiss. 2012. Single Molecule Quantum-Confined Stark Effect Measurements of Semiconductor Nanoparticles at Room Temperature. ACS Nano 6:10013-10023.